BioID screening of biotinylation sites using the avidin-like protein Tamavidin 2-REV identifies global interactors of stimulator of interferon genes (STING)

Received for publication, May 12, 2020, and in revised form, June 15, 2020 Published, Papers in Press, June 17, 2020, DOI 10.1074/jbc.RA120.014323

Kou Motani and Hideteka Kosako*

From the Division of Cell Signaling, Fujii Memorial Institute of Medical Sciences, Tokushima University, Tokushima, Japan

Edited by Roger J. Colbran

Stimulator of interferon genes (STING) mediates cytosolic DNA-induced innate immune signaling via membrane trafficking. The global identification of proteins that spatiotemporally interact with STING will provide a better understanding of its trafficking mechanisms and of STING signaling pathways. Proximity-dependent biotin identification (BioID) is a powerful technology to identify physiologically relevant protein-protein interactions in living cells. However, biotinylated peptides are rarely detected in the conventional BioID method, which uses streptavidin beads to pull down biotinylated proteins, because the biotin-streptavidin interaction is too strong. As a result, only nonbiotinylated peptides are identified, which cannot be distinguished from peptides of nonspecifically pull-downed proteins. Here, we developed a simple method to efficiently and specifically enrich biotinylated peptides using Tamavidin 2-REV, an engineered avidin-like protein with reversible biotin-binding capability. Using RAW264.7 macrophages stably expressing TurboID-fused STING, we identified and quantified >4,000 biotinylated peptides of STING-proximal proteins. Various endoplasmic reticulum-associated proteins were biotinylated in unstimulated cells, and STING activation caused biotinylation of many proteins located in the Golgi and endosomes. These proteins included those known to interact with activated STING, such as TANK-binding kinase 1 (TBK1), several palmitoyl transferases, and p62/sequestosome 1 (SQSTM1). Furthermore, interferon-induced transmembrane protein 3 (IFITM3), an endolysosome-localized antiviral protein, bound to STING at the late activation stage. These dynamic interaction profiles will provide detailed insights into STING signaling; we propose that our approach using Tamavidin 2-REV would be useful for BioID-based and other biotinylation-based peptide identification methods.

The presence of pathogenic or self-DNA in the cytosol is a danger signal that triggers the host innate immune system and leads to the production of cyclic GMP-AMP (cGAMP) (1–4). cGAMP functions as a second messenger that binds to and activates the adaptor protein STING, which consists of a four-pass transmembrane domain at the N terminus and a cytosolic cGAMP-binding domain at the C terminus (5–8). Upon binding to cGAMP, inactive dimeric STING undergoes a conformational change, forms oligomers (9–11), and translocates from the endoplasmic reticulum (ER) to the Golgi apparatus (12), where STING is palmitoylated (13) and causes recruitment and activation of the serine/threonine kinase TANK-binding kinase 1 (TBK1) (10). Activated TBK1 then phosphorylates the transcription factor interferon regulatory factor 3 (IRF3) to induce the expression of type I interferon (IFN) and chemokine genes (14, 15). After activation at the Golgi, STING moves to endosomes and then to lysosomes, where STING is ubiquitinated and recruits the autophagy receptor p62/sequestosome 1 (SQSTM1) that leads to the degradation of STING to prevent the excessive production of IFN (16–18). To understand the molecular mechanisms of how the STING pathway is tightly regulated by membrane trafficking, it is important to globally identify proteins that spatiotemporally interact with STING in living cells.

BioID is a unique and powerful technique to identify transiently or indirectly interacting proteins in living cells, and it is based on the use of the biotin ligase BirA with promiscuous R118G mutation (19). When a protein of interest fused to this ligase is expressed in cells, it biotinylates lysine residues of proximal proteins (20–22). The identification of biotinylated proteins usually has been performed by pulldown with streptavidin beads followed by LC-MS/MS analysis (23–25). However, biotinylated peptides are rarely detected in this conventional method because of the extremely high affinity of streptavidin for biotin. As a result, mostly nonbiotinylated peptides are identified, and they cannot be distinguished from peptides of nonspecifically pull-downed contaminating proteins.

To overcome this problem, two groups have recently reported an elegant approach using anti-biotin antibodies to enrich and identify biotinylated peptides from proteolytic digests of cellular proteins (26, 27). This new strategy enables mapping of biotinylation sites on proteins and provides spatial and topological information about proteins and protein complexes. However, elution of biotinylated peptides from the antibodies requires harsh conditions (*e.g.* TFA), which may increase the contamination of nonbiotinylated peptides.

In this study, we have improved the BioID method to efficiently and specifically enrich biotinylated peptides by using Tamavidin 2-REV, an engineered avidin-like protein with reversible biotin-binding capability. Two avidin-like proteins, Tamavidin 1 and Tamavidin 2, were previously isolated from the Tamogitake mushroom (28), and one point mutation (S36A) was introduced into Tamavidin 2 to break the hydrogen bond between Tamavidin 2 and biotin (29). This engineered Tamavidin 2, named Tamavidin 2-REV, reversibly bound to biotinylated peptides, which could be mildly and specifically

This article contains supporting information.

* For correspondence: Hideteka Kosako, kosako@tokushima-u.ac.jp.

eluted by the addition of excess biotin. By using immobilized Tamavidin 2-REV beads, over 4,000 biotinylated peptides were identified and quantified from cells stably expressing STING fused to TurboID (30). Whereas the biotinylation of various ER proteins was detected in unstimulated cells, STING activation caused the biotinylation of many proteins localized in the Golgi and endosomes. These proteins included previously known and unknown interactors of activated STING. The STING interactome obtained in this study will provide new insights into the STING signaling network, and our approach using Tamavidin 2-REV would enable researchers to utilize BioID and other identification methods based on protein biotinylation more easily and effectively.

Results

TurboID enables short-time biotin labeling of STING-proximal proteins

Recently, Ting and coworkers developed TurboID, which can catalyze proximity biotinylation with much greater efficiency than the original BioID (30). To compare these biotin ligase variants fused to STING in cells, the original BioID (BirA*) fused to the C terminus or the N terminus of STING or TurboID (BirA**) fused to the N terminus of STING (Fig. 1*A*) was stably expressed in STING-null (SKO) RAW264.7 macrophages. When these cells were incubated with biotin for various times, the biotinylation of many cellular proteins was quickly and strongly detected by Western blotting in cells expressing TurboID-STING (Fig. 1*B*). When DMXAA, a cell-permeable artificial STING ligand (7, 31), was added to STING-null RAW264.7 cells, phosphorylation of TBK1 was not detected (Fig. 1*C*). However, DMXAA-induced phosphorylation of TBK1 was rescued by ectopic expression of either FLAG-tagged STING or TurboID-STING (Fig. 1*C*), indicating that TurboID-fused STING is functional. When TurboID-STING-expressing cells were treated with or without DMXAA for 1 h in the presence of biotin, biotinylation of many proteins in both stimulated and unstimulated cells was detected by Western blotting (Fig. 1*D*). To observe TurboID-STING-mediated protein biotinylation *in situ*, TurboID-STING-expressing cells were treated with or without DMXAA for 1 h in the presence of biotin, fixed, and stained with fluorescent streptavidin. In unstimulated cells, both V5-tagged TurboID-STING and biotinylated proteins exhibited a mesh-like distribution throughout the cytoplasm, which is consistent with the ER localization of STING at the steady state (Fig. 1*E*, *left*). On the other hand, DMXAA stimulation caused the accumulation of both TurboID-STING and biotinylated proteins in a Golgi-like perinuclear region, where STING is known to translocate from the ER after its activation (Fig. 1*E*, *right*). These results indicate that STING-fused TurboID can quickly and strongly biotinylate STING-proximal proteins in unstimulated and stimulated cells.

Specific enrichment of biotinylated peptides using Tamavidin 2-REV is useful for the BioID screen

An approach using anti-biotin antibodies for enrichment and identification of biotinylated peptides has been developed recently by two groups (26, 27). We reasoned that biotinylated peptides could be more specifically and efficiently enriched by Tamavidin 2-REV with reversible biotin-binding capability (29). Total proteins from control or DMXAA-treated (for 1 h in the presence of biotin in three biological replicates) TurboID-STING-expressing cells were digested with trypsin, and biotinylated peptides were directly captured on immobilized Tamavidin 2-REV beads without the cumbersome process of peptide purification (Fig. 2*A*). Protease resistance of Tamavidin 2-REV (29) is suited for direct incubation with digested peptide solutions containing trypsin. The bound biotinylated peptides were eluted with excess free biotin followed by LC-MS/MS and label-free quantification. In total, we identified and quantified 5149 peptides, 4021 (78%) of which were biotinylated peptides (Fig. 2*B*, Table S1). When biotinylated peptides in the same tryptic digests were captured on anti-biotin antibody beads, LC-MS/MS analysis of the eluates with TFA identified and quantified 11,534 peptides, 2795 (24%) of which were biotinylated peptides (Fig. 2*B*, Table S2). Most (74%) of these biotinylated peptides were also identified by enrichment with Tamavidin 2-REV (Fig. 2*C*). Thus, Tamavidin 2-REV enables large-scale identification of biotinylated peptides from BioID samples.

Quantification of biotinylated peptides of STING-proximal proteins

We compared the Tamavidin 2-REV-enriched biotinylated peptides between control and DMXAA-treated TurboID-STING-expressing cells (Fig. 3*A*, Table S1). As expected, biotinylation of TBK1 was significantly increased by DMXAA stimulation (Fig. 3*A*). In addition, biotinylation of SQSTM1 was also increased by DMXAA stimulation (Fig. 3*A*). Gene ontology analysis revealed that biotinylation of ER-related proteins was decreased by DMXAA stimulation (Fig. 3*B*, *left*). On the other hand, biotinylation of Golgi- and endosome-related proteins and proteins involved in vesicle-mediated transport processes was increased by DMXAA stimulation (Fig. 3*B*, *right*). These STING interactome profiles are consistent with the activation-induced STING trafficking, in which activated STING is transported from the ER through the Golgi apparatus to endosomes (12, 18).

Interestingly, biotinylation of several putative ZDHHC-type palmitoyl transferases (32) was increased by DMXAA stimulation (Table S1). These ZDHHC proteins are known to be localized in the Golgi (33) and may be involved in the palmitoylation of STING at the Golgi (13). As shown in Fig. S1, treatment with the palmitoylation inhibitor 2-bromopalmitate (2-BP) suppressed DMXAA-induced phosphorylation of TBK1 and IRF3 in RAW264.7 cells, as reported previously in other cell types (13). This confirms the importance of palmitoylation in STING signaling in RAW264.7 macrophages.

Although STING is known to interact with IRF3 to promote the TBK1-mediated phosphorylation of IRF3 (14, 15), biotinylation of IRF3 was not detected in TurboID-STING-expressing cells (Tables S1 and S2). In contrast, several biotinylated peptides of IRF5 were significantly increased by DMXAA stimulation (Fig. 3*A*). To examine whether STING activation causes TBK1-mediated phosphorylation of IRF5, RAW264.7 cells were treated with DMXAA in the presence or absence of the TBK1 inhibitor BX795, and cell lysates were subjected to

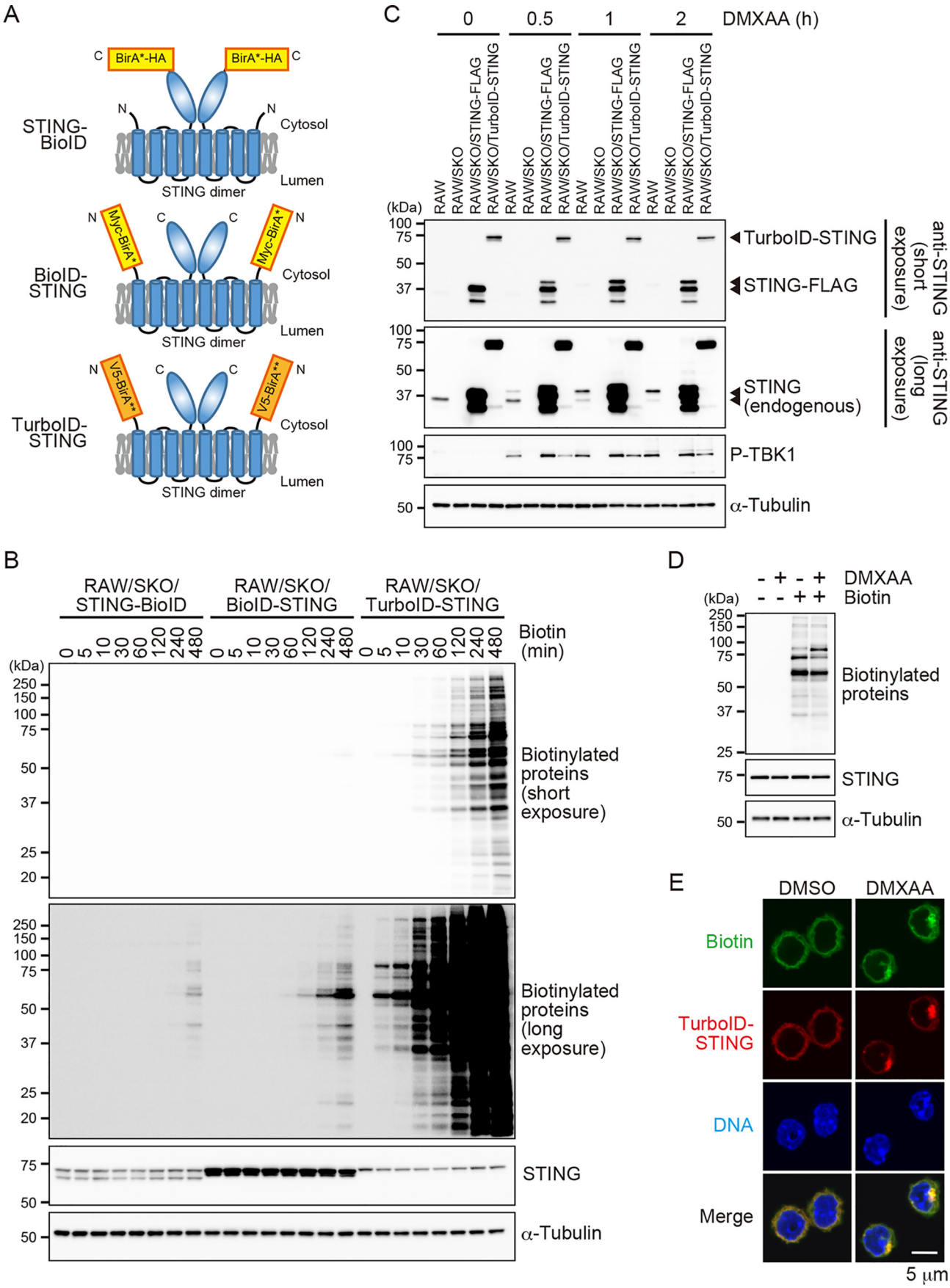
A
STING-BioID
BirA*-HA
BirA*-HA
Cytosol
Lumen
STING dimer
BioID-STING
Myc-BirA*
Myc-BirA*
Cytosol
Lumen
STING dimer
TurboID-STING
V5-BirA**
V5-BirA**
Cytosol
Lumen
STING dimer
C
0
0.5
1
2
DMXAA (h)
RAW
RAW/SKO
RAW/SKO/STING-FLAG
RAW/SKO/TurboID-STING
(kDa)
TurboID-STING
STING-FLAG
anti-STING (short exposure)
STING (endogenous)
anti-STING (long exposure)
P-TBK1
α-Tubulin
B
RAW/SKO/ STING-BioID
RAW/SKO/ BioID-STING
RAW/SKO/ TurboID-STING
Biotin (min)
0 5 10 30 60 120 240 480
(kDa)
Biotinylated proteins (short exposure)
Biotinylated proteins (long exposure)
STING
α-Tubulin
D
DMXAA
Biotin
(kDa)
Biotinylated proteins
STING
α-Tubulin
E
DMSO
DMXAA
Biotin
TurboID-STING
DNA
Merge
5 μm

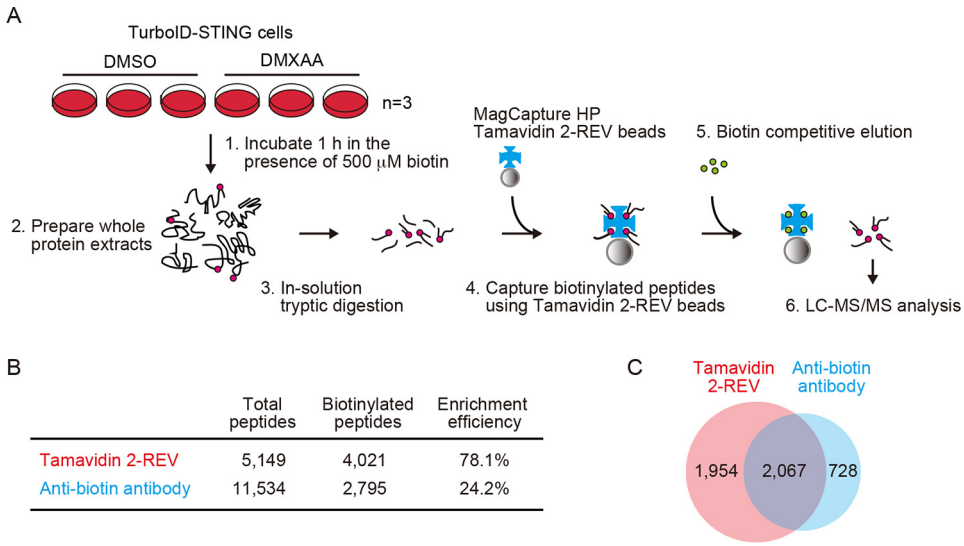

	Total peptides	Biotinylated peptides	Enrichment efficiency
Tamavidin 2-REV	5,149	4,021	78.1%
Anti-biotin antibody	11,534	2,795	24.2%

Figure 2. Comparison of Tamavidin 2-REV-based enrichment and antibody-based enrichment for identification of biotinylated peptides. *A*, schematic workflow of enrichment and identification of biotinylated peptides using Tamavidin 2-REV, which has reversible biotin-binding capability. Three biological replicates for each sample were analyzed by LC-MS/MS analysis. *B*, the number of total peptides and biotinylated peptides that were identified and quantified by LC-MS/MS analysis. *C*, overlap of biotinylated peptides identified and quantified using Tamavidin 2-REV-based enrichment or anti-biotin antibody-based enrichment.

phosphate affinity (Phos-tag) SDS-PAGE (34), followed by Western blotting with anti-IRF5 antibody. As shown in Fig. 4*A*, DMXAA stimulation induced an electrophoretic mobility shift of IRF5. This mobility shift was reversed by treatment of the cell lysates with lambda protein phosphatase (Fig. 4*B*), confirming that the shift is caused by phosphorylation. Furthermore, the DMXAA-induced shift of IRF5 was blocked by pretreatment with BX795 (Fig. 4*C*), indicating that IRF5 is phosphorylated by the STING-TBK1 pathway.

IFITM3 interacts with STING at the late activation stage

Among the newly identified STING-proximal proteins, we focused on IFITM3 because of its important role in antiviral defense (35–38). DMXAA stimulation induced biotinylation of IFITM3 at K24 in the N-terminal region and K88 in the middle region (Figs. 3*A* and 5*A*). Although early studies reported IFITM3 as a two-pass transmembrane protein with luminal N and C termini, recent studies have proposed a new topology with a cytosolic N terminus and a luminal C terminus (39, 40). Because STING-fused TurboID localizes to the cytosol (Fig. 1*A*), biotinylation of IFITM3 in the N-terminal region supports the latter topology model.

To observe the trafficking-dependent association between STING and IFITM3, we established RAW264.7 cells stably expressing GFP-fused STING and analyzed colocalization of GFP-STING with IFITM3. Endogenous IFITM3 was localized to an endolysosome-like perinuclear region (36) regardless of STING activation status and did not colocalize with GFP-STING at the steady state (Fig. 5*B*). Upon DMXAA stimulation, GFP-STING was accumulated in the IFITM3-positive compartments (Fig. 5*B*, *arrows*). It should be noted that DMXAA also induced the formation of STING aggregates, possibly SQSTM1-positive compartments (17, 18), where IFITM3 was hardly detected (Fig. 5*B*, *arrowheads*). To further examine the interaction between STING and IFITM3, lysates from GFP-STING-expressing cells were immunoprecipitated with anti-GFP nanobody-coupled beads, followed by Western blotting with anti-IFITM3 antibody. The interaction between STING and IFITM3 was gradually increased from 1 to 4 h after DMXAA stimulation (Fig. 5, *C* and *D*). In contrast, DMXAA stimulation induced phosphorylation of TBK1 at 1 h, and this phosphorylation was diminished by 4 h (Fig. 5*C*). IFITM3 was also coimmunoprecipitated with endogenous STING from lysates of DMXAA-stimulated RAW264.7 cells (Fig. 5*E*). The amount of coimmunoprecipitated IFITM3 was increased at 4 h after DMXAA stimulation, although endogenous STING protein was strongly reduced at 4 h (Fig. 5*E*). These results define IFITM3 as a novel STING interactor at the late activation stage.

Discussion

In this study, we have developed a simple and easy method for enrichment and identification of biotinylated peptides using Tamavidin 2-REV. To date, other avidin- or streptavidin-derived artificial proteins that were designed to bind biotin

Figure 1. Biotin labeling of STING-proximal proteins. *A*, schematic of the BioID and TurboID fusion proteins. *B*, STING-null (SKO) RAW264.7 cells expressing STING-BioID, BioID-STING, or TurboID-STING were cultured in the presence of 500 μM biotin for the indicated times. The cell lysates were analyzed by Western blotting with HRP-conjugated streptavidin and antibodies to STING and α-tubulin. *C*, WT RAW264.7 cells, STING-null RAW264.7 cells, or STING-null RAW264.7 cells expressing either STING-FLAG or TurboID-STING were treated with 30 μg/ml DMXAA for the indicated times. The cell lysates were analyzed by Western blotting with antibodies to STING, phospho-TBK1, and α-tubulin. *D*, TurboID-STING-expressing cells were treated with DMSO (−) or 30 μg/ml DMXAA for 1 h in the presence or absence of 500 μM biotin. The cell lysates were analyzed by Western blotting with HRP-conjugated streptavidin and antibodies to STING and α-tubulin. *E*, TurboID-STING-expressing cells were treated with DMSO or 100 μg/ml DMXAA for 1 h in the presence of biotin, fixed, and stained with DyLight 488-conjugated streptavidin, anti-V5 antibody, and DAPI, followed by observation under a confocal microscope. Scale bar, 5 μm.

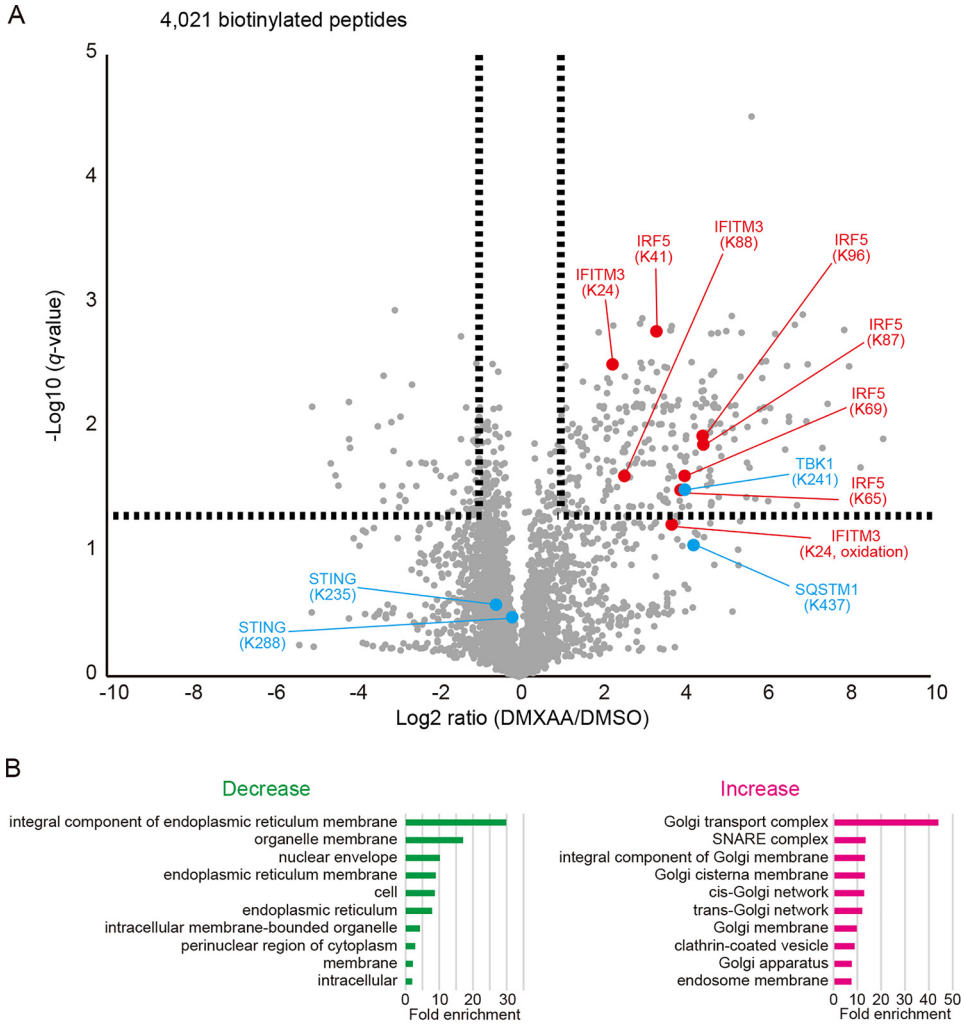

Figure 3. Activation-induced changes in STING-proximal proteins. *A*, volcano plot showing differential peptide profiles in DMSO- and DMXAA (30 μg/ml)-treated TurboID-STING-expressing cells. Identified and quantified biotinylated peptides are plotted as $\log_2$ fold change (DMXAA/DMSO) *versus* negative $\log_{10}$ of the *t* test *q* value. Biotinylated peptides of known interactors of activated STING and STING itself are shown in *blue*, and those of unknown STING interactors are shown in *red*. *B*, enrichment analysis of the ontology for proteins of biotinylated peptides that decreased (*left*) or increased (*right*) after DMXAA stimulation.

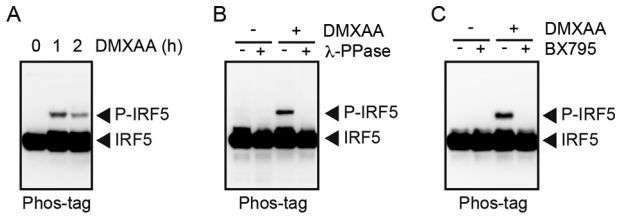

Figure 4. IRF5 is phosphorylated by TBK1 upon STING activation. IRF5 phosphorylation in cell lysates was analyzed by Phos-tag Western blotting with anti-IRF5 antibody. *A*, RAW264.7 cells were stimulated with 30 μg/ml DMXAA for the indicated times. *B*, RAW264.7 cells were treated with DMSO (−) or 30 μg/ml DMXAA for 1 h. The cell lysates were incubated with or without λ protein phosphatase (λ-PPase) before Western blotting. *C*, RAW264.7 cells were pretreated with or without 1 μM BX795 for 30 min and then treated with DMSO or 30 μg/ml DMXAA for 1 h. Representative data are shown from three (*A*) or two (*B* and *C*) independent experiments.

reversibly have been reported (29), such as nitro-avidin (41), streptavidn-S45A (42), and streptavidin-M4 (43). However, Tamavidin 2-REV has several advantages over these other proteins for enrichment and MS-based identification of biotinylated peptides. First, protease resistance of Tamavidin 2-REV is suited for direct incubation with digested peptides containing proteases, such as trypsin, without peptide purification. Second, the neutral pI (pI 7.4) of Tamavidin 2-REV is expected to reduce charge-derived nonspecific binding. Third, Tamavidin 2-REV can be highly expressed as a soluble protein in *E. coli* and does not tend to aggregate.

Enrichment of biotinylated peptides from complex peptide mixtures greatly increases identification of biotinylation sites compared with streptavidin-based enrichment of biotinylated proteins (26, 27). Tamavidin 2-REV-based enrichment of biotinylated peptides is a time- and cost-effective method compared with antibody-based enrichment. Whereas elution of biotinylated peptides from anti-biotin antibodies requires harsh conditions, biotinylated peptides can be specifically eluted from Tamavidin 2-REV by adding excess free biotin under mild conditions. In fact, enrichment efficiency using Tamavidin 2-REV was over 3-fold higher than that using anti-biotin antibody (Fig. 2*B*), which may have another disadvantage of lot-to-lot variation. Thus, enrichment of biotinylated peptides using Tamavidin 2-REV followed by identification of biotinylation sites by LC-MS/MS would be useful for a wide range of applications that require biotinylation of proteins. These applications

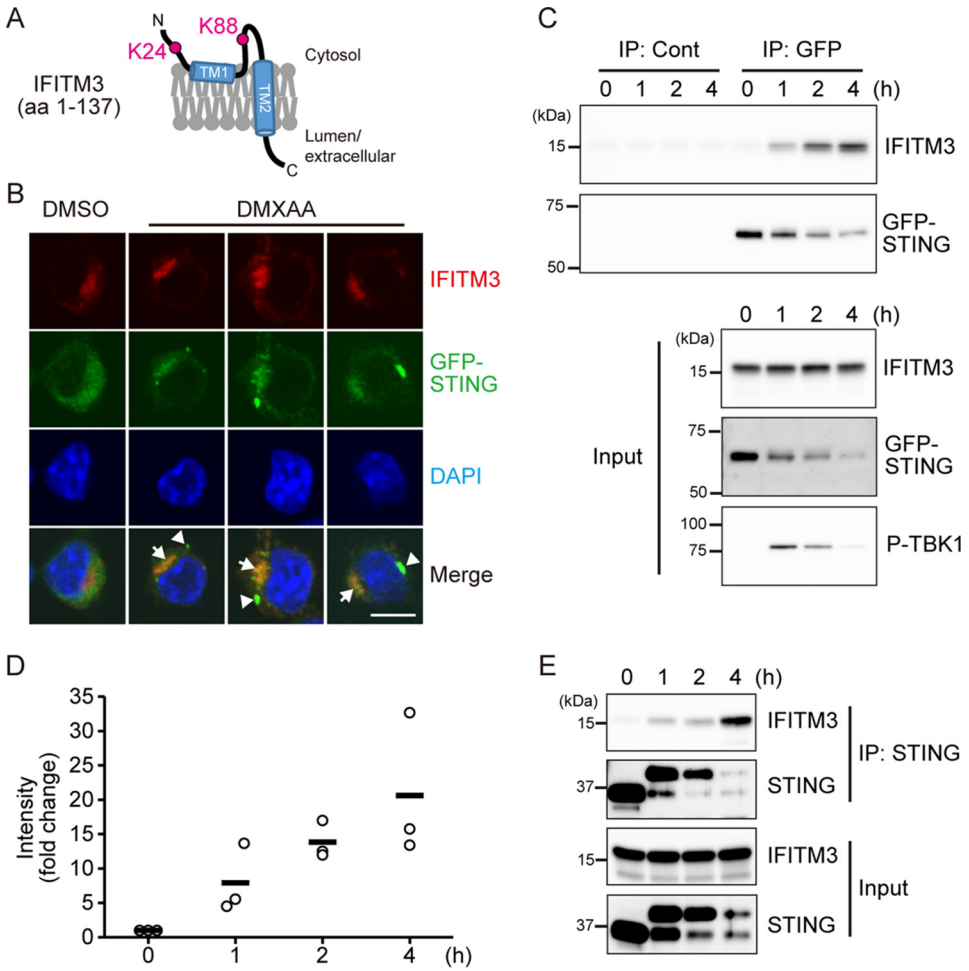

Figure 5. Activation-induced interaction between STING and IFITM3. *A*, protein structure and topology of IFITM3 with biotinylation sites are shown. *TM*, transmembrane domain. *B*, RAW264.7 cells expressing GFP-STING (RAW/GFP-STING cells) were treated with DMSO or 100 μg/ml DMXAA for 4 h. The cells were fixed and stained with anti-IFITM3 antibody and DAPI, followed by observation under a confocal microscope. *Scale bar*, 5 μm. *C*, RAW/GFP-STING cells were treated with 30 μg/ml DMXAA for the indicated times. The cells were lysed and immunoprecipitated with anti-Spot tag nanobody-coupled magnetic agarose beads (Spot-Trap_MA, control) or anti-GFP nanobody-coupled magnetic agarose beads (GFP-Trap_MA), followed by Western blotting with antibodies to IFITM3, GFP, and phospho-TBK1. *D*, the band intensities of IFITM3 immunoprecipitated with GFP-Trap_MA were quantified using the Image Laboratory software (n = 3). A scatter plot with the mean value line is shown. *E*, RAW264.7 cells were treated with or without 30 μg/ml DMXAA for the indicated times. The cells were lysed and immunoprecipitated with anti-STING antibody, followed by Western blotting with antibodies to IFITM3 and STING. Representative data are shown from two (*B* and *E*) or three (*C*) independent experiments.

include proximity labeling (BioID and APEX [44]), cell surface labeling, cross-linking MS (45), and mapping sites of posttranslational modifications (PTMs), such as palmitoylation (46), *S*-nitrosylation, sulfenylation, and *O*-GlcNAc modification (27).

It is well known that IRF3 is the major transcription factor downstream of the STING-TBK1 pathway. Although the reason why biotinylation of IRF5 but not IRF3 was detected is unclear, it may be because of markedly higher expression of IRF5 protein in RAW264.7 cells than other cell lines tested (Fig. S2). Whereas S396 of IRF3 is phosphorylated by TBK1 to induce its nuclear translocation and gene expression, S462 of IRF5, a position equivalent to that of S396 of IRF3, is not phosphorylated by TBK1 but is phosphorylated by IKKβ (47, 48). Detailed mechanisms and functions of the STING-TBK1-mediated phosphorylation of IRF5 remain to be elucidated in the future.

In the BioID screen using TurboID-fused STING, we identified the endolysosomal antiviral protein IFITM3 as a novel STING interactor. Because IFITM3 has been reported to have redundant functions with IFITM1 and IFITM2 (35, 38, 39), we generated triple knockout (TKO) RAW264.7 cells lacking IFITM1, IFITM2, and IFITM3 (Fig. S3*A*). However, the TKO cells and WT cells exhibited similar kinetics of phosphorylation of TBK1 and degradation of STING after DMXAA stimulation (Fig. S3*B*). Although the physiological role of the STING–IFITM3 interaction remains unclear, STING showed increased binding to IFITM3 concomitant with decreased phosphorylation of TBK1 at the late activation stage (Fig. 5, *C* and *E*), suggesting that TBK1 and IFITM3 have different roles in STING signaling. IFITM3 is an antiviral restriction factor especially against enveloped RNA viruses, including influenza A virus, West Nile virus, dengue virus, and Zika virus (35–38). Whereas STING is known to be essential for IFN response against DNA viruses, accumulating evidence suggests that STING also restricts the replication of such RNA viruses through undefined mechanisms (49–52). Thus, STING might regulate the antiviral activity of IFITM3. Future studies need to clarify the role of the STING-IFITM3 axis on antiviral immune responses.

Experimental procedures

Reagents and antibodies

MagCapture HP Tamavidin 2-REV magnetic beads and 2-bromohexadecanoic acid (2-BP) were purchased from FUJIFILM Wako Pure Chemical (Osaka, Japan). HRP-conjugated streptavidin and DyLight 488-conjugated streptavidin were purchased from BioLegend (San Diego, CA). Anti-V5 mAb (M215-3) and anti-GFP pAb (598) were from MBL (Nagoya, Japan). Anti-IFITM3 pAb (ab15592) and anti-IRF5 mAb (ab181553) were from Abcam (Cambridge, United Kingdom). The PTMScan anti-biotin kit (41343), anti-STING mAb (13647), and anti-phospho-TBK1 (Ser172) mAb (5483) were from Cell Signaling Technology (Danvers, MA). GFP-Trap_MA and Spot-Trap_MA (for immunoprecipitation) were from ChromoTek (Planegg-Martinsried, Germany). DMXAA was from Ark Pharm, Inc. (Arlington Heights, IL). D-biotin was from Nacalai Tesque (Kyoto, Japan).

Cell lines

RAW264.7 murine macrophage cells were cultured in DMEM containing 10% FCS. STING-deficient RAW264.7 cells and the STING-deficient cells stably expressing FLAG-tagged STING were generated previously (53). To generate cells expressing TurboID-STING fusion protein, V5-TurboID (Addgene) followed by 2× GGGGS flexible linker was fused to the N terminus of mouse STING. Classical BioID was also fused to the N terminus or C terminus of mouse STING, inserting the linker between them. These fusion constructs were stably introduced into the STING-deficient RAW264.7 cells using the PiggyBac transposon vector (54) kindly gifted by Dr. Yasuhide Ohinata (Chiba University). After puromycin treatment, the bulk of the resistant cells was used in this study. To generate cells expressing GFP-STING fusion protein, EGFP followed by 2× GGGGS linker was fused to the N terminus of mouse STING and introduced into the pEF-BOS vector. After transfection by electroporation using the NEPA21 system (Nepagene, Chiba, Japan), a single clone was obtained by limiting dilution. To generate IFITM1/2/3 TKO cells, the px330 vector (Addgene) expressing Cas9 and single guide RNA targeting for mouse IFITM1, IFITM2, and IFITM3 (5′-AGGGACCAGACCACATGGTC-3′) and EGFP expression vector were cotransfected into RAW264.7 cells by electroporation using the NEPA21 system. After 48 h of incubation at 37 °C, the cells strongly expressing EGFP were sorted by an S3e Cell Sorter (Bio-Rad, Hercules, CA) and subjected to limiting dilution, and the mutated clones were identified by Western blotting and DNA sequencing.

Preparation of cell lysates and immunoprecipitates

For preparing total cell lysates, cells were directly lysed in 1× SDS sample buffer (40 mM Tris-HCl [pH 6.8], 2% SDS, 5% glycerol, 1% β-mercaptoethanol, and 0.01% bromphenol blue) and heated at 95 °C for 10 min. For immunoprecipitation assay, cells were lysed in NP-40 lysis buffer (20 mM Tris-HCl [pH 7.5], 150 mM NaCl, 1 mM EDTA, 1% NP-40, and 10% glycerol) supplemented with a protease inhibitor mixture (Nacalai Tesque), a phosphatase inhibitor mixture (Nacalai Tesque), and 50 units/ml Benzonase nuclease (Merck Millipore, Burlington, MA). After incubation on ice for 10 min, the lysates were centrifuged at 20,000 × *g* for 15 min at 4 °C. The supernatants were incubated with Spot-Trap_MA, GFP-Trap_MA, or anti-STING antibody-coupled Protein G Mag-Sepharose (GE Healthcare, Little Chalfont, United Kingdom) at 4 °C for 3 h. After washing with the NP-40 lysis buffer four times, the beads were resuspended in 1× SDS sample buffer and heated at 95 °C for 10 min.

SDS-PAGE and Western blotting

Total cell lysates and immunoprecipitates were separated by electrophoresis on a 10% or 16% (for IFITM3) polyacrylamide gel and transferred onto a PVDF membrane (Merck Millipore). After blocking, the membrane was incubated with primary antibodies in 5% skim milk overnight at 4 °C, followed by incubation with HRP-conjugated secondary antibodies. Protein bands on the membrane were detected by a ChemiDoc Touch Imaging System (Bio-Rad) after incubation of the membrane with Clarity Western ECL substrate (Bio-Rad) or ImmunoStar LD (FUJIFILM Wako). For Phos-tag Western blotting, cells were lysed in 6 M guanidine-HCl containing 100 mM HEPES-NaOH (pH 7.5) and 2 mM DTT, followed by protein precipitation using a PAGE Clean-up kit (Nacalai Tesque). After dissolving in 1× SDS sample buffer, SDS-PAGE was performed using a gel containing 25 μM Phos-tag acrylamide (FUJIFILM Wako) and 50 μM $MnCl_2$ as described previously (55). For treatment with lambda protein phosphatase (λ-PPase), cell lysates were concentrated and buffer exchanged into 1× NEB λ-PPase buffer (New England Biolabs, Ipswich, MA) using Amicon Ultra 30K (Merck Millipore). The samples were incubated with 4000 units/ml λ-PPase (New England Biolabs) in the presence of 1 mM $MnCl_2$ for 30 min at 30 °C. All Western blotting experiments were repeated at least twice, and representative images are shown.

Immunostaining

Cells were seeded on coverslips in a 12-well plate. After treatment with DMSO or DMXAA, the cells were fixed with 3.7% formaldehyde–PBS for 15 min at 37 °C and permeabilized with 0.2% Triton X-100–PBS for 10 min at room temperature. The coverslips were incubated with primary antibodies in 2% goat serum–PBS for 1 h at 37 °C. After washing with PBS three times, the coverslips were incubated with Alexa Fluor-conjugated secondarily antibodies and 4′,6-diamidino-2-phenylindole dihydrochloride (DAPI) for 1 h at room temperature in the dark. After washing with PBS three times and subsequent rinse with distilled water, the coverslips were mounted on the glass slides with FluorSave reagent (Merck Millipore). The immunofluorescence images were obtained by an FV1200 confocal laser scanning microscope (Olympus, Tokyo, Japan). All immunostaining experiments were repeated at least twice, and representative images are shown.

Sample preparation for the BioID screen

The STING-null RAW264.7 cells expressing TurboID-STING were seeded in 15-cm dishes and cultured overnight. The cells were treated with DMSO or 30 μg/ml DMXAA, and

biotin (final concentration of 500 μM) was added to the medium. After 1 h of incubation, the cells were washed with HEPES-buffered saline twice and lysed in 6 M guanidine-HCl containing 100 mM HEPES-NaOH (pH 7.5), 10 mM Tris (2-carboxyethyl) phosphine, and 40 mM chloroacetamide. The lysates were dissolved by heating and sonication and then centrifuged at 20,000 × *g* for 15 min at 4 °C. The supernatants were recovered, and proteins (3.4 mg each) were purified by methanol–chloroform precipitation and solubilized by 0.1% RapiGest SF (Waters, Milford, MA) in 50 mM triethylammonium bicarbonate. After repeated sonication and vortexing, the proteins were digested with 34 μg trypsin (MS grade, Thermo Fisher Scientific, Waltham, MA) at 37 °C overnight. The resultant peptide solutions were diluted 5-fold with TBS (50 mM Tris-HCl [pH 7.5] and 150 mM NaCl) and divided in half for enrichment using Tamavidin 2-REV or anti-biotin antibody.

Enrichment of biotinylated peptides using Tamavidin 2-REV

Biotinylated peptides from the BioID samples were captured on 15 μl slurry of MagCapture HP Tamavidin 2-REV magnetic beads in the presence of 1 mg/ml Pefabloc SC (Sigma-Aldrich) during 3 h of incubation at 4 °C. After washing with TBS five times, the biotinylated peptides were eluted with 100 μl of 1 mM biotin in TBS for 15 min at 95 °C twice. The combined eluates were desalted using GL-Tip SDB (GL Sciences, Tokyo, Japan), evaporated in a SpeedVac concentrator (Thermo Fisher Scientific), and redissolved in 0.1% TFA and 3% acetonitrile (ACN).

Enrichment of biotinylated peptides using anti-biotin antibody

Biotinylated peptides from the BioID samples were captured on 20 μl slurry of the anti-biotin (A7C2A) rabbit mAb-conjugated beads (41343, Cell Signaling Technology) in the presence of 1 mg/ml Pefabloc SC during 3 h of incubation at 4 °C. After washing with TBS four times and with ultrapure water twice, the biotinylated peptides were eluted with 100 μl of 0.2% TFA in 80% ACN for 10 min at room temperature twice. The combined eluates were evaporated, dissolved in 0.1% TFA, and desalted using GL-Tip SDB. The desalted eluates were further evaporated and redissolved in 0.1% TFA and 3% ACN.

Data-dependent LC-MS/MS analysis

LC-MS/MS analysis of the resultant peptides was performed on an EASY-nLC 1200 UHPLC connected to a Q Exactive Plus mass spectrometer through a nanoelectrospray ion source (Thermo Fisher Scientific). The peptides were separated on a 75-μm-inner-diameter, 150-mm C_{18} reversed-phase column (Nikkyo Technos, Tokyo, Japan) with a linear 4–32% ACN gradient for 0–60 min, followed by an increase to 80% ACN for 10 min. The mass spectrometer was operated in data-dependent acquisition mode with a top 10 MS/MS method. MS1 spectra were measured with a resolution of 70,000, an AGC target of 1×10^6, and a mass range from 350 to 1,500 *m/z*. MS/MS spectra were triggered at a resolution of 17,500, an AGC target of 5×10^4, an isolation window of 2.0 *m/z*, a maximum injection time of 200 ms, and a normalized collision energy of 27. Dynamic exclusion was set to 15 s. Raw data were directly analyzed against the Swiss-Prot database, version 2017-10-25, restricted to *Mus musculus* (25,097 sequences) using Proteome Discoverer version 2.4 (Thermo Fisher Scientific) with the Sequest HT search engine. The search parameters were the following: (*a*) trypsin as an enzyme with up to two missed cleavages; (*b*) precursor mass tolerance of 10 ppm; (*c*) fragment mass tolerance of 0.02 Da; (*d*) carbamidomethylation of cysteine as a fixed modification; and (*e*) acetylation of protein N terminus, oxidation of methionine, and biotinylation of lysine as variable modifications. Peptides were filtered at a false discovery rate (FDR) of 1% using the Percolator node of Proteome Discoverer. Label-free quantification was performed based on intensities of precursor ions using the Precursor Ions Quantifier node. Normalization was performed such that the total sum of abundance values for each sample over all peptides was the same. The data were analyzed by a two-tailed Student's *t* test, and the resulting *p* values were adjusted using the Benjamini-Hochberg method for controlling the FDR (56). A volcano plot was used for showing the mean fold change and *q* value (FDR-adjusted *p* value) of each biotinylated peptide.

Gene ontology enrichment analysis

The lists of proteins of differentially biotinylated peptides before and after STING activation in the BioID screen (fold change of >2, *q* value of <0.05) were analyzed using DAVID Bioinformatics Resources version 6.8 (count threshold, >4; Benjamin-corrected *p* value, <0.05). Top 10 enriched gene ontology terms of cellular components are shown.

Data availability

The MS proteomics data have been deposited in the ProteomeXchange Consortium via the jPOST partner repository with the data set identifiers PXD018802 and PXD018803 (57).

Acknowledgments—We thank Dr. Yasuhide Ohinata for kindly providing the PiggyBac vector. We thank Drs. Tatsuya Saitoh, Takumi Koshiba, and Tomohiko Taguchi for helpful comments. We also thank Mayumi Kajimoto and Megumi Kawano for technical assistance and Mayumi Iwata for secretarial assistance.

Author contributions—K. M. resources; K. M. and H. K. data curation; K. M. and H. K. formal analysis; K. M. and H. K. funding acquisition; K. M. validation; K. M. and H. K. investigation; K. M. visualization; K. M. and H. K. project administration; K. M. and H. K. writing-review and editing; H. K. conceptualization; H. K. supervision; H. K. methodology; H. K. writing-original draft.

Funding and additional information—This work was supported by the JSPS KAKENHI (grant numbers 17K08661 and 20K07340) and the Takeda Science Foundation (to K. M.) and by the JSPS KAKENHI (grant numbers 18KK0229, 19H04966, and 20K06628) and the Japan Foundation for Applied Enzymology (to H. K.).

Conflict of interest—The authors declare that they have no conflicts of interest with the contents of this article.

Abbreviations—The abbreviations used are: STING, stimulator of interferon genes; ER, endoplasmic reticulum; BioID, proximity-dependent biotin identification; TBK1, TANK-binding kinase 1;

SQSTM1, sequestosome 1; IFITM3, interferon-induced transmembrane protein 3; cGAMP, cyclic GMP-AMP; IRF3, interferon regulatory factor 3; IFN, interferon; DMXAA, 5, 6-dimethylxanthenone-4-acetic acid; TFA, trifluoroacetic acid; 2-BP, 2-bromopalmitate; ACN, acetonitrile; APEX, engineered ascorbate peroxidase; PTM, post-translational modification; FDR, false discovery rate; DAPI, 4′,6-diamidino-2-phenylindole dihydrochloride.

References

1. Wu, J., Sun, L., Chen, X., Du, F., Shi, H., Chen, C., and Chen, Z. J. (2013) Cyclic GMP-AMP is an endogenous second messenger in innate immune signaling by cytosolic DNA. *Science* **339,** 826–830 CrossRef Medline
2. Sun, L., Wu, J., Du, F., Chen, X., and Chen, Z. J. (2013) Cyclic GMP-AMP synthase is a cytosolic DNA sensor that activates the type I interferon pathway. *Science* **339,** 786–791 CrossRef Medline
3. Ablasser, A., Goldeck, M., Cavlar, T., Deimling, T., Witte, G., Röhl, I., Hopfner, K. P., Ludwig, J., and Hornung, V. (2013) cGAS produces a 2′-5′-linked cyclic dinucleotide second messenger that activates STING. *Nature* **498,** 380–384 CrossRef Medline
4. Ablasser, A., and Chen, Z. J. (2019) cGAS in action: expanding roles in immunity and inflammation. *Science* **363,** eaat8657 CrossRef
5. Ishikawa, H., and Barber, G. N. (2008) STING is an endoplasmic reticulum adaptor that facilitates innate immune signalling. *Nature* **455,** 674–678 CrossRef Medline
6. Ishikawa, H., Ma, Z., and Barber, G. N. (2009) STING regulates intracellular DNA-mediated, type I interferon-dependent innate immunity. *Nature* **461,** 788–792 CrossRef Medline
7. Gao, P., Ascano, M., Zillinger, T., Wang, W., Dai, P., Serganov, A. A., Gaffney, B. L., Shuman, S., Jones, R. A., Deng, L., Hartmann, G., Barchet, W., Tuschl, T., and Patel, D. J. (2013) Structure-function analysis of STING activation by c[G(2′,5′)pA(3′,5′)p] and targeting by antiviral DMXAA. *Cell* **154,** 748–762 CrossRef Medline
8. Motwan, M., Pesiridis, S., and Fitzgerald, K. A. (2019) DNA sensing by the cGAS-STING pathway in health and disease. *Nat. Rev. Genet.* **20,** 657–674 CrossRef Medline
9. Shang, G., Zhang, C., Chen, Z. J., Bai, X. C., and Zhang, X. (2019) Cryo-EM structures of STING reveal its mechanism of activation by cyclic GMP-AMP. *Nature* **567,** 389–393 CrossRef Medline
10. Zhang, C., Shang, G., Gui, X., Zhang, X., Bai, X. C., and Chen, Z. J. (2019) Structural basis of STING binding with and phosphorylation by TBK1. *Nature* **567,** 394–398 CrossRef Medline
11. Ergun, S. L., Fernandez, D., Weiss, T. M., and Li, L. (2019) STING polymer structure reveals mechanisms for activation, hyperactivation, and inhibition. *Cell* **178,** 290–301 CrossRef Medline
12. Saitoh, T., Fujita, N., Hayashi, T., Takahara, K., Satoh, T., Lee, H., Matsunaga, K., Kageyama, S., Omori, H., Noda, T., Yamamoto, N., Kawai, T., Ishii, K., Takeuchi, O., Yoshimori, T., *et al.* (2009) Atg9a controls dsDNA-driven dynamic translocation of STING and the innate immune response. *Proc. Natl. Acad. Sci. U S A* **106,** 20842–20846 CrossRef Medline
13. Mukai, K., Konno, H., Akiba, T., Uemura, T., Waguri, S., Kobayashi, T., Barber, G. N., Arai, H., and Taguchi, T. (2016) Activation of STING requires palmitoylation at the Golgi. *Nat. Commun.* **7,** 11932 CrossRef Medline
14. Tanaka, Y., and Chen, Z. J. (2012) STING specifies IRF3 phosphorylation by TBK1 in the cytosolic DNA signaling pathway. *Sci. Signal.* **5,** ra20 CrossRef Medline
15. Liu, S., Cai, X., Wu, J., Cong, Q., Chen, X., Li, T., Du, F., Ren, J., Wu, Y. T., Grishin, N. V., and Chen, Z. J. (2015) Phosphorylation of innate immune adaptor proteins MAVS, STING, and TRIF induces IRF3 activation. *Science* **347,** aaa2630 CrossRef Medline
16. Gonugunta, V. K., Sakai, T., Pokatayev, V., Yang, K., Wu, J., Dobbs, N., and Yan, N. (2017) Trafficking-mediated STING degradation requires sorting to acidified endolysosomes and can be targeted to enhance anti-tumor response. *Cell Rep.* **21,** 3234–3242 CrossRef Medline
17. Prabakaran, T., Bodda, C., Krapp, C., Zhang, B-C., Christensen, M. H., Sun, C., Reinert, L., Cai, Y., Jensen, S. B., Skouboe, M. K., Nyengaard, J. R., Thompson, C. B., Lebbink, R. J., Sen, G. C., Loo, G., *et al.* (2018) Attenuation of cGAS-STING signaling is mediated by a p62/SQSTM1-dependent autophagy pathway activated by TBK1. *EMBO J.* **37,** e97858 CrossRef
18. Taguchi, T., and Mukai, K. (2019) Innate immunity signalling and membrane trafficking. *Curr. Opin. Cell Biol.* **59,** 1–7 CrossRef Medline
19. Roux, K. J., Kim, D. I., Raida, M., and Burke, B. (2012) A promiscuous biotin ligase fusion protein identifies proximal and interacting proteins in mammalian cells. *J. Cell Biol.* **196,** 801–810 CrossRef Medline
20. Kim, D. I., and Roux, K. J. (2016) Filling the void: proximity-based labeling of proteins in living cells. *Trends Cell Biol.* **26,** 804–817 CrossRef Medline
21. Varnaitė, R., and MacNeill, S. A. (2016) Meet the neighbors: mapping local protein interactomes by proximity-dependent labeling with BioID. *Proteomics* **16,** 2503–2518 CrossRef Medline
22. Gingras, A.-C., Abe, K. T., and Raught, B. (2019) Getting to know the neighborhood: using proximity-dependent biotinylation to characterize protein complexes and map organelles. *Curr. Opin. Chem. Biol.* **48,** 44–54 CrossRef Medline
23. Gupta, G. D., Coyaud, É., Gonçalves, J., Mojarad, B. A., Liu, Y., Wu, Q., Gheiratmand, L., Comartin, D., Tkach, J. M., Cheung, S. W. T., Bashkurov, M., Hasegan, M., Knight, J. D., Lin, Z.-Y., Schueler, M., *et al.* (2015) A dynamic protein interaction landscape of the human centrosome-cilium interface. *Cell* **163,** 1484–1499 CrossRef Medline
24. Uezu, A., Kanak, D. J., Bradshaw, T. W. A., Soderblom, E. J., Catavero, C. M., Burette, A. C., Weinberg, R. J., and Soderling, S. H. (2016) Identification of an elaborate complex mediating postsynaptic inhibition. *Science* **353,** 1123–1129 CrossRef Medline
25. Yoshinaka, T., Kosako, H., Yoshizumi, T., Furukawa, R., Hirano, Y., Kuge, O., Tamada, T., and Koshiba, T. (2019) Structural basis of mitochondrial scaffolds by prohibitin complexes: insight into a role of the coiled-coil region. *iScience* **19,** 1065–1078 CrossRef Medline
26. Udeshi, N. D., Pedram, K., Svinkina, T., Fereshetian, S., Myers, S. A., Aygun, O., Krug, K., Clauser, K., Ryan, D., Ast, T., Mootha, V. K., Ting, A. Y., and Carr, S. A. (2017) Antibodies to biotin enable large-scale detection of biotinylation sites on proteins. *Nat. Methods* **14,** 1167–1170 CrossRef Medline
27. Kim, D. I., Cutler, J. A., Na, C. H., Reckel, S., Renuse, S., Madugundu, A. K., Tahir, R., Goldschmidt, H. L., Reddy, K. L., Huganir, R. L., Wu, X., Zachara, N. E., Hantschel, O., and Pandey, A. (2018) BioSITe: a method for direct detection and quantification of site-specific biotinylation. *J. Proteome Res.* **17,** 759–769 CrossRef Medline
28. Takakura, Y., Tsunashima, M., Suzuki, J., Usami, S., Kakuta, Y., Okino, N., Ito, M., and Yamamoto, T. (2009) Tamavidins—novel avidin-like biotin-binding proteins from the Tamogitake mushroom. *FEBS J.* **276,** 1383–1397 CrossRef Medline
29. Takakura, Y., Sofuku, K., and Tsunashima, M. (2013) Tamavidin 2-REV: an engineered tamavidin with reversible biotin-binding capability. *J. Biotechnol.* **164,** 19–25 CrossRef Medline
30. Branon, T. C., Bosch, J. A., Sanchez, A. D., Udeshi, N. D., Svinkina, T., Carr, S. A., Feldman, J. L., Perrimon, N., and Ting, A. Y. (2018) Efficient proximity labeling in living cells and organisms with TurboID. *Nat. Biotech.* **36,** 880–887 CrossRef Medline
31. Conlon, J., Burdette, D. L., Sharma, S., Bhat, N., Thompson, M., Jiang, Z., Rathinam, V. A. K., Monks, B., Jin, T., Xiao, T. S., Vogel, S. N., Vance, R. E., and Fitzgerald, K. A. (2013) Mouse, but not human STING, binds and signals in response to the vascular disrupting agent 5,6-dimethylxanthenone-4-acetic acid. *J. Immunol.* **190,** 5216–5225 CrossRef Medline
32. Fukata, M., Fukata, Y., Adesnik, H., Nicoll, R. A., and Bredt, D. S. (2004) Identification of PSD-95 palmitoylating enzymes. *Neuron* **44,** 987–996 CrossRef Medline
33. Ernst, A. M., Syed, S. A., Zaki, O., Bottanelli, F., Zheng, H., Hacke, M., Xi, Z., Rivera-Molina, F., Graham, M., Rebane, A. A., Björkholm, P., Baddeley, D., Toomre, D., Pincet, F., and Rothman, J. E. (2018) S-palmitoylation sorts membrane cargo for anterograde transport in the Golgi. *Dev. Cell* **47,** 479–493 CrossRef Medline

34. Kinoshita, E., Kinoshita-Kikuta, E., Takiyama, K., and Koike, T. (2006) Phosphate-binding tag, a new tool to visualize phosphorylated proteins. *Mol. Cell. Proteomics* **5,** 749–757 CrossRef Medline
35. Brass, A. L., Huang, I.-C., Benita, Y., John, S. P., Krishnan, M. N., Feeley, E. M., Ryan, B. J., Weyer, J. L., van der Weyden, L., Fikrig, E., Adams, D. J., Xavier, R. J., Farzan, M., and Elledge, S. J. (2009) The IFITM proteins mediate cellular resistance to influenza A H1N1 virus, West Nile virus, and dengue virus. *Cell* **139,** 1243–1254 CrossRef Medline
36. Feeley, E. M., Sims, J. S., John, S. P., Chin, C. R., Pertel, T., Chen, L.-M., Gaiha, G. D., Ryan, B. J., Donis, R. O., Elledge, S. J., and Brass, A. L. (2011) IFITM3 inhibits influenza A virus infection by preventing cytosolic entry. *PLoS Pathog.* **7,** e1002337 CrossRef Medline
37. Amini-Bavil-Olyaee, S., Choi, Y. J., Lee, J. H., Shi, M., Huang, I.-C., Farzan, M., and Jung, J. U. (2013) The antiviral effector IFITM3 disrupts intracellular cholesterol homeostasis to block viral entry. *Cell Host Microbe* **13,** 452–464 CrossRef Medline
38. Savidis, G., Perreira, J. M., Portmann, J. M., Meraner, P., Guo, Z., Green, S., and Brass, A. L. (2016) The IFITMs inhibit Zika virus replication. *Cell Rep.* **15,** 2323–2330 CrossRef Medline
39. Bailey, C. C., Zhong, G., Huang, I.-C., and Farzan, M. (2014) IFITM-family proteins: the cell's first line of antiviral defense. *Annu. Rev. Virol.* **1,** 261–283 CrossRef Medline
40. Ling, S., Zhang, C., Wang, W., Cai, X., Yu, L., Wu, F., Zhang, L., and Tian, C. (2016) Combined approaches of EPR and NMR illustrate only one transmembrane helix in the human IFITM3. *Sci. Rep.* **6,** 24029 CrossRef Medline
41. Morag, E., Bayer, E. A., and Wilchek, M. (1996) Reversibility of biotin-binding by selective modification of tyrosine in avidin. *Biochem. J.* **316,** 193–199 CrossRef
42. Hyre, D. E., Stayton, P. S., Trong, I. L., Freitag, S., and Stenkamp, R. E. (2000) Ser45 plays an important role in managing both the equilibrium and transition state energetics of the streptavidin-biotin system. *Protein Sci.* **9,** 878–885 CrossRef Medline
43. Wu, S.-C., and Wong, S.-L. (2005) Engineering soluble monomeric streptavidin with reversible biotin binding capability. *J. Biol. Chem.* **280,** 23225–23231 CrossRef Medline
44. Lam, S. S., Martell, J. D., Kamer, K. J., Deerinck, T. J., Ellisman, M. H., Mootha, V. K., and Ting, A. Y. (2015) Directed evolution of APEX2 for electron microscopy and proximity labeling. *Nat. Methods* **12,** 51–54 CrossRef Medline
45. Petrotchenko, E. V., Serpa, J. J., and Borchers, C. H. (2011) An isotopically coded CID-cleavable biotinylated cross-linkers for structural proteomics. *Mol. Cell. Proteomics* **10,** M110.001420 CrossRef Medline
46. Wan, J., Roth, A. F., Bailey, A. O., and Davis, N. G. (2007) Palmitoylated proteins: purification and identification. *Nat. Protoc.* **2,** 1573–1584 CrossRef Medline
47. Lopez-Pelaez, M., Lamont, D. J., Peggie, M., Shpiro, N., Gray, N. S., and Cohen, P. (2014) Protein kinase IKKβ-catalyzed phosphorylation of IRF5 at Ser462 induces its dimerization and nuclear translocation in myeloid cells. *Proc. Natl. Acad. Sci. U S A* **111,** 17432–17437 CrossRef Medline
48. Ren, J., Chen, X., and Chen, Z. J. (2014) IKKβ is a IRF5 kinase that instigates inflammation. *Proc. Natl. Acad. Sci. U S A* **111,** 17438–17443 CrossRef Medline
49. Aguirre, S., Maestre, A. M., Pagni, S., Patel, J. R., Savage, T., Gutman, D., Maringer, K., Bernal-Rubio, D., Shabman, R. S., Simon, V., Rodriguez-Madoz, J. R., Mulder, L. C. F., Barber, G. N., and Fernandez-Sesma, A. (2012) DENV inhibits type I IFN production in infected cells by cleaving human STING. *PLoS Pathog.* **8,** e1002934 CrossRef Medline
50. You, F., Wang, P., Yang, L., Yang, G., Zhao, Y. O., Qian, F., Walker, W., Sutton, R., Montgomery, R., Lin, R., Iwasaki, A., and Fikrig, E. (2013) ELF4 is critical for induction of type I interferon and the host antiviral response. *Nat. Immunol.* **14,** 1237–1246 CrossRef Medline
51. Holm, C. K., Rahbek, S. H., Gad, H. H., Bak, R. O., Jakobsen, M. R., Jiang, Z., Hansen, A. L., Jensen, S. K., Sun, C., Thomsen, M. K., Laustsen, A., Nielsen, C. G., Severinsen, K., Xiong, Y., Burdette, D. L., *et al.* (2016) Influenza A virus targets a cGAS-independent STING pathway that controls enveloped RNA viruses. *Nat. Commun.* **7,** 10680 CrossRef Medline
52. Franz, K. M., Neidermyer, W. J., Tan, Y.-J., Whelan, S. P. J., and Kagan, J. C. (2018) STING-dependent translation inhibition restricts RNA virus replication. *Proc. Natl. Acad. Sci. U S A* **115,** E2058–E2067 CrossRef Medline
53. Motani, K., and Kosako, H. (2018) Activation of stimulator of interferon genes (STING) induces ADAM17-mediated shedding of the immune semaphoring SEMA4D. *J. Biol. Chem.* **293,** 7717–7726 CrossRef Medline
54. Matsui, H., Fujimoto, N., Sasakawa, N., Ohinata, Y., Shima, M., Yamanaka, S., Sugimoto, M., and Hotta, A. (2014) Delivery of full-length factor VIII using a piggyBac transposon vector to correct a mouse model of hemophilia A. *PLoS ONE* **9,** e104957 CrossRef Medline
55. Kosako, H. (2009) Phos-tag Western blotting for detecting stoichiometric protein phosphorylation in cells. *Protocol Exchange* CrossRef
56. Benjamini, Y., and Hochberg, Y. (1995) Controlling the false discovery rate: a practical and powerful approach to multiple testing. *J. R. Stat. Soc. B* **57,** 289–300 CrossRef
57. Okuda, S., Watanabe, Y., Moriya, Y., Kawano, S., Yamamoto, T., Matsumoto, M., Takami, T., Kobayashi, D., Araki, N., Yoshizawa, A. C., Tabata, T., Sugiyama, N., Goto, S., and Ishihama, Y. (2017) jPOSTrepo: an international standard data repository for proteomes. *Nucleic Acids Res.* **45,** D1107–D1111 CrossRef Medline